Localization with Guaranteed Bound on the Position Error using a Drone *

Cristina M. Pinotti
Univ. of Perugia, Italy
cristina.pinotti@unipg.it

Francesco Betti Sorbelli
Univ. of Florence, Italy
francesco.bettisorbelli@unifi.it

Pericle Perazzo
Univ. of Pisa, Italy
pericle.perazzo@iet.unipi.it

Gianluca Dini
Univ. of Pisa, Italy
gianluca.dini@iet.unipi.it

ABSTRACT

In this paper, we study the sensor localization problem using a drone. Our goal is to localize each sensor in the deployment area ensuring a predefined localization precision, i.e., a bound on the position error, whatever is the drone's altitude. We show how to guarantee a-priori the precision localization by satisfying few conditions. Such conditions are totally novel aspects that have not been considered in previous localization algorithms.

In the new localization technique, we first determine the minimum ground distance that guarantees the predefined bound on the position error. According to that distance, a static path for the drone is designed. Then, the localization mission proceeds in two steps: Initially, the drone computes a rough estimation of the sensor position by using the first three distance measurements it can take greater than the minimum ground distance. Next the position is refined by employing three distance measurements that, in addition to the minimum ground distance, satisfy a specific geometric layout. In this way, the localization precision is guaranteed with just three measurements.

Keywords

guaranteed localization precision; drone; altitude; collinearity; localization mission; static path.

*The work has been partially supported by the European project "Geospatial based Environment for Optimization Systems Addressing Fire Emergencies" (GEO-SAFE), contract no. H2020-691161, and by the Italian project "RISE: un nuovo framework distribuito per data collection, monitoraggio e comunicazioni in contesti di emergency response", Fondazione Cassa Risparmio Perugia, code 2016.0104.021.

1. INTRODUCTION

One of the first critical research issue in wireless sensor networks (WSNs) is to determine the physical locations of nodes on the ground.

Many existing localization algorithms require a large number of anchor nodes, i.e., nodes whose position is known a-priori [7, 16, 17]. In the literature, localization algorithms that use mobile anchor nodes have been considered to decrease the cost associated with the deployment of multiple anchors and to maximize the localization accuracy [10]. The use of mobile nodes has also been encouraged by the recent advances in technology in the area of small unmanned aerial systems, commonly known as drones [15]. One must be aware, however, that specific problems occur planning the localization mission for drones that fly at a certain altitude.Indeed, when the drone is in plumb-line with the node to be measured, a small imprecision on the line-of-sight (3D) distance between the drone and the node will translate into a very big error on their ground (2D) distance. Such an error increases with the drone's altitude.

To the best of our knowledge, no previous work on localization has given the bound of the position error as function of the drone's altitude. In this paper, we express the localization precision as function of the node-drone ground distance, of the drone altitude, and of the geometry of the ranging waypoints; and we propose a drone localization technique able to guarantee any predefined localization precision.

In this work, we assume that the drone can measure its altitude with negligible error. A technology allowing for such precise altitude measurements is Differential GPS (DGPS) [8]. We also assume that the drone infers the distance measurements from the round-trip time of messages exchanged with the nodes on the ground. Finally, to compute the position of each non-localized node, the drone performs a trilateration method and returns the least-squares-error solution as the estimated position.

Our Results.

- We prove by geometric considerations a bound on the position error which reflects the drone's altitude, the drone-node ground distance, and the geometry of the ranging waypoints (see Section 2). At the best of our knowledge, such a bound is totally new;

- We design a new localization technique for flying anchors (see Sections 3): Our solution guarantees a predefined bound on the position error by tuning a single parameter;
- We experimentally evaluate our algorithm showing that for a random deployment of sensors and for different altitudes the predefined bound on the position error is always satisfied; The gap between the experimental bound on the position error and the predefined bound is of the order of centimeters, especially at high altitudes (see Section 4).

1.1 Related Work

Drone-based localization of ground devices has been studied in [3–5, 12]. One of the most emblematic approaches is the one given in [4] where a robot sweeps the entire area and periodically broadcasts its GPS position. The nodes collect such messages, called position broadcasts. The nodes finally infer their own position by averaging all the received position broadcasts. In our localization technique, the drone computes the node position. Nonetheless, no one of these works consider either the ground error due to the altitude of the drone or the bound on the position error.

Another problem that uses static paths to sweep the deployment area is drone-based data gathering from sensors [2,6].In this case, a robot (either aerial, terrestrial, or underwater) must collect data from a set of sparse and unconnected sensors. These papers propose path planning algorithms that solve generalized forms of the Traveler Salesman Problem (TSP). The objective is usually to minimize the path length while respecting particular constraints. While a single waypoint per sensor is sufficient for data gathering, for sensor localization at least three distinct waypoints are required for each sensor.

In [13], a path planning algorithm based on TSP is proposed, instead, to securely verify the positions of a set of devices.

Different trajectories that a mobile anchor (not necessary a flying drone) can follow in order to localize a set of sensor nodes are proposed in [9,10]. Although these works were not interested in bounding the position error, they were interested in avoiding to select collinear waypoints for performing the distance measurements for the same node. In Section 4, we compare the bound of the position error of our technique with that in [10].

Organization.

The rest of the paper is organized as follows: Section 2 proves a bound on the position error based on geometric considerations. Section 3 describes the localization technique and proves that it can be tuned to guarantee whatever predefined localization precision. A large set of experiments is presented in Section 4. Finally, Section 5 offers some conclusions and future work.

2. LOCALIZATION PRECISION

We consider an area Q of size $Q_x \times Q_y$ and a set of sensors randomly deployed in Q that we want to localize using a drone that flies at a non-negligible altitude h_{max}. The drone regularly sends a message beacon as it moves and the ground nodes that can hear the beacon reply with an ack message to the drone. From the round-trip time, the drone infers the distance between itself and the node. For measuring the round-trip time, we assume that the drone employs impulse-radio ultra-wideband (IR-UWB) technology, which has a measurement precision of the order of centimeters [1, 11].

The positions along the path where the drone sends the beacons and takes the distance measurements are called *waypoints*. The waypoints from which a node P is measured are called the *ranging waypoints* of P and are denoted as $w_1(P), w_2(P), \ldots, w_m(P)$. The ground is assumed to be flat enough to allow the drone to be always in the line of sight with the node to be measured. We define the *communication range* $r = \min(r_{node}, r_{drone})$ as the minimum between the communication range $r_{\texttt{drone}}$ of the drone and the communication range $r_{\texttt{node}}$ of the node. When the drone measures a node, it measures the *slant distance* s, that is, the line-of-sight distance between the drone and the node. Hence, the slant distance s cannot be greater than the communication range r.

We assume that the slant distance measurements can be subject to errors that depend on the employed technology for reception of the messages. Our provable bound on the position error is guaranteed up to a bound on the slant distance error, called the *slant precision* ϵ_s. Moderate changes in the drone position, for example due to the sudden wind impact, can also be tolerated by our localization technique as the localization precision holds up to a maximum altitude h_{max}, starting from a minimum node-drone ground distance d_{min}, and up to a maximum interwaypoint distance. Moreover, when needed, for example because there are chances that the altitude or the ground distance are not respected, the drone can recompute its position during the mission.

A localization algorithm aims to determine for each sensor P in Q its physical location after collecting a small number of slant distances of P. Assuming that the communication range is r and that the altitude is at most h_{max}, than the drone can measure nodes up to ground distance:

$$d_{max} = \sqrt{r^2 - h_{max}^2}. \quad (1)$$

From now on, let the ground precision ϵ_d and the localization precision ϵ_L be the upper bounds on the ground distance error and on the position error, respectively. They are both always worse than the slant precision. Especially if the waypoints are badly laid out with respect to the node, small errors in the slant distances will translate into big errors on the ground. Examples of bad layouts are *collinearity among the ranging waypoints* (i.e., three of more waypoints that measure the same node are on the same line) and *waypoint collinearity with the node to be localized* (i.e., at least two waypoints and the point to be measured are almost on the same line, see Fig. 1). If the waypoints are collinear amongst themselves, the trilateration identifies two positions, a real one and an "alias" one, both measured with the same precision. To avoid the "alias" problem, it is sufficient to never perform trilateration from three collinear waypoints. Instead, to measure the waypoint collinearity with the node, we introduce the *angular aperture*, which is the minimum angle $\beta(P)$ formed by the node-waypoint directions at P. In Fig. 1, $\beta(P)$ is the angle $\widehat{w_2(P)Pw_3(P)}$. A smaller angular aperture means a greater collinearity with the node.

Having collected at least three slant distance measurements for each non-localized node, the drone can determine the positions of the node by performing trilateration. The

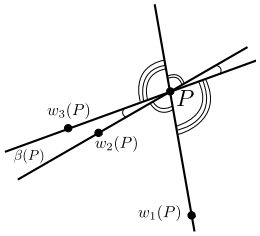

Figure 1: Angular aperture $\beta(P)$.

trilateration method, however, applies to the ground distances. Hence, the drone needs to translate the slant-distance measurement $s(w, P)$ between its position in altitude w and the node P into the *ground distance* $d(w', P)$ between the *projection* w' of w on the ground and P. The drone easily computes the ground distance $d(w', P) = \sqrt{s(w, P)^2 - h^2}$, where h is the drone altitude. Note that $d(w', P)$ denotes the ground distance measurement and, as such, it is subject to a ground error e_d that depends on the slant error e_s. We call *slant precision* ϵ_s the maximum absolute value[1] of the slant error and, since we assume the drone uses the IR-UWB technology, ϵ_s is of order of centimeters [1]. Moreover, as we mostly refer in our description to the projection of the waypoints on the ground, with a little abuse of notation, from now on, we denote both the waypoint in altitude w and its projection w' on the ground with w if it is clear from the context to which one we refer.

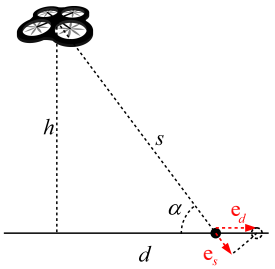

Figure 2: Relationship between slant error e_s and the ground error e_d.

Note that if all the ground distances and the slant distances are sufficiently large compared to the ground error and the slant error, then the measurement circumferences of the trilateration are linearizable at the node position, without changing significantly the problem solution. In this way, the measurement circumferences are approximated with measurement lines, which are perpendicular to the waypoint-node direction (see Fig. 2 and 3).

As shown in Fig. 2, the error e_d on the ground distance is $e_s \cdot \frac{1}{\cos(\alpha)} = e_s \cdot \sqrt{1 + (h/d)^2}$, where α is the angle of incidence of the slant distance to the ground, d is the actual ground distance, h is the actual drone's altitude, and e_s is the actual error on the measured slant distance. Thus, if every measured node is at actual ground distance at least $d \geq d_{min}$ from the ranging waypoint and the drone altitude is at most h_{max}, than the maximum absolute value of the

[1] For all the precisions in this paper, we give the maximum absolute value.

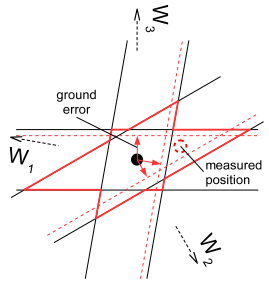

Figure 3: Measurement lines forming a "star" shape. The dashed red lines are the measurement lines. The black solid lines are the measurement lines when the ground error is maximum, i.e., $e_d = \pm\epsilon_d$.

ground error, called the *ground precision* ϵ_d becomes:

$$\epsilon_d = \epsilon_s \sqrt{1 + \frac{h_{max}^2}{d_{min}^2}}. \tag{2}$$

Once the ground measures $d(w_1, P)$, $d(w_2, P)$, and $d(w_3, P)$ have been computed for a node P from the ranging waypoint $w_1 = (x_{w_1}, y_{w_1})$, $w_2 = (x_{w_2}, y_{w_2})$ and $w_3 = (x_{w_3}, y_{w_3})$, the drone performs a trilateration to estimate the node position. Due to the ground errors, the three measurement lines that approximate the waypoint-node circles do not intersect at a single point: Each different pair of measurement lines intersects at a point; The three intersection points, one for each different pair of the three measurement lines, delimit a small area (see Fig. 3) which contains the position determined by the last-squares-error method. The red "star" in Fig. 3 is the area that contains the estimated position P_t whatever is the ground error of the three measurement lines associated with the three measures taken for node P.

The estimated position $P_t = (x, y)$ is the point that minimizes:

$$\begin{aligned} &\min \quad \delta_1^2 + \delta_2^2 + \delta_3^2 \\ \text{s.t.} \quad &\sqrt{(x_{w_i} - x)^2 + (y_{w_i} - y)^2} + \delta_i = d(w_i, P) \\ &\qquad\qquad for \quad i = 1, 2, 3. \end{aligned} \tag{3}$$

The maximum absolute value of the position error, called

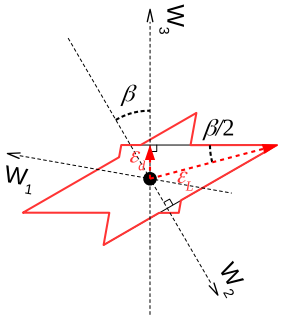

Figure 4: Relationship between ground precision ϵ_d and localization precision ϵ_L.

localization precision ϵ_L, occurs when the estimated position is at the furthest vertex of the "star" shape. In Fig. 4, the furthest vertex of the "star" occurs at the intersection point

of the two measurements lines approximating the circumferences of radius $d(P, w_3)$ and $d(P, w_2)$ when the absolute value of the ground error is ϵ_d. The angle centered at such intersection point has width β because it is the supplemental angle of the angle formed in P by the waypoint-node direction starting at w_3 and at w_2. Thus, by elementary geometric considerations, the maximum error in Fig 4 is $\frac{\epsilon_d}{\sin(\frac{\beta}{2})}$. Repeating the same reasoning for all the 12 vertices of the "star", one can see that the distance of the vertices of the "star" from P is either $\frac{\epsilon_d}{\cos(\frac{\beta}{2})}$ or $\frac{\epsilon_d}{\sin(\frac{\beta}{2})}$ where β varies among the angles in which the turn angle at P is partitioned by the waypoint-node directions. Since we have proved that the furthest vertex of the "star" is at distance $\frac{\epsilon_d}{\sin(\frac{\beta(P)}{2})}$ [14] where $\beta(P)$ is the angular aperture, then:

$$\epsilon_L = \frac{\epsilon_d}{\sin(\frac{\beta_{min}}{2})} = \epsilon_s \cdot \frac{\sqrt{1 + (h_{max}/d_{min})^2}}{\sin(\frac{\beta_{min}}{2})} \quad (4)$$

where β_{min} is the minimum angular aperture among all the nodes in Q.

3. THE LOCALIZATION TECHNIQUE

In this section, we present a localization technique that uses a static path to sweep Q and that guarantees an a-priori given localization precision ϵ_L.

3.1 Provable Bound on Position Error

From now on, we call the distance between every two consecutive waypoints I_w and we fix

$$\frac{\beta_{min}}{2} = \tan^{-1}\left(\frac{\frac{d_{min}}{2}}{\sqrt{3}\frac{d_{min}}{2} + 2I_w}\right). \quad (5)$$

We say that any node P is *correctly* measured if the drone can choose on its path three ranging waypoints $w_1(P), w_2(P)$ and $w_3(P)$ for P that satisfy the following constraints:

1. constraint d_{max} : $d(w_i(P), P) \leq d_{max}$, for $1 \leq i \leq 3$;
2. constraint d_{min} : $d(w_i(P), P) \geq d_{min}$, for $1 \leq i \leq 3$;
3. constraint β_{min} : $\beta(P) \geq \beta_{min}$.

By Eq. 4 and Eq. 5, a localization technique that *correctly* measures all the nodes in Q guarantees:

$$\epsilon_L = \epsilon_s \frac{\sqrt{(1 + \frac{h_{max}^2}{d_{min}^2})(1 + \tan^2(\frac{\beta_{min}}{2}))}}{\tan(\frac{\beta_{min}}{2})}. \quad (6)$$

Now suppose we want design a localization mission that guarantees an a-priori fixed localization precision ϵ_L. Assuming that the communication range r, the altitude h_{max}, the interwaypoint distance I_w, and the slant precision ϵ_s are fixed a-priori because of legal restrictions or technical reasons, d_{max} and β_{min} follow from Eq. 1 and Eq. 5. Then, the unique free parameter in Eq. 6 is d_{min}, which can be tuned so as the a-priori required localization precision is obtained for all the nodes in Q.

Table 1 lists d_{min} values analytically derived by Eq. 6 for standard values of h_{max} and possible values of I_w, fixing $\epsilon_s = 0.10\ m$. As one can see, a smaller localization precision requires larger values of d_{min}. The same precision can be pursued for increasing values of I_w choosing larger values of d_{min}.

		$\epsilon_L(m)$	0.3	0.6	0.9	1.2
h_{max} (m)	$I_w(m)$					
160	2		149.28	60.30	39.87	30.30
	5		158.35	65.39	44.30	34.38
	10		173.12	72.98	50.60	39.99
90	2		86.63	35.44	23.76	18.28
	5		95.55	40.14	27.72	21.84
	10		110.02	46.88	33.09	26.52

Table 1: The values d_{min} that satisfy ϵ_L values. All the measures are in meters.

Now, we will describe the new localization technique assuming we know the value d_{min} required to guarantee the desired precision ϵ_L. In the next section, we start by describing the static path $\mathcal{D}$ that the drone will follow during the localization. This is a simple scan path which has been adapted in order to correctly measure all the nodes of Q.

3.2 Static Path $\mathcal{D}$

The static path $\mathcal{D}$ consists of vertical scans connected by horizontal scan, as depicted in Fig. 5. The waypoints belong only to the vertical scans of $\mathcal{D}$. The distance between two consecutive waypoints is fixed to I_w. The waypoints along the vertical scans are numbered bottom-up, starting from 0. We say that a waypoint is *even* if it gets an even number. Each vertical scan continues beyond the top and down borders for a segment of length $F_y = (d_{max} - I_w)\frac{\sqrt{3}}{2}$ and it is rounded to start and finish with an even waypoint. Thus, each vertical scan has length $L = 2I_w \left\lceil \frac{Q_y + 2F_y}{2I_w} \right\rceil$. Two consecutive vertical scans are connected by a horizontal segment of length $H = (d_{max} - d_{min} - 2I_w)\frac{1}{2}$. Let H be termed the *inter-scan* distance. The drone traverses one vertical scan of $\mathcal{D}$ bottom-up and the next one top-down. The horizontal segments are traversed from left to right (see Fig. 5). The starting point of $\mathcal{D}$ is $S = (s_x, s_y) = (-F_x - H, -F_y)$, where $F_x = \frac{d_{min}}{2}$. From the starting point, we can take correct measurements for the bottom left corner of Q. Note that neither F_x or H are rounded to be a multiple of I_w because there are no waypoints on the horizontal segments of $\mathcal{D}$. The path $\mathcal{D}$ consists of two vertical scans outside Q that are used to measure the nodes in the leftmost stripe of Q, followed by several vertical scan inside Q. The last vertical scan

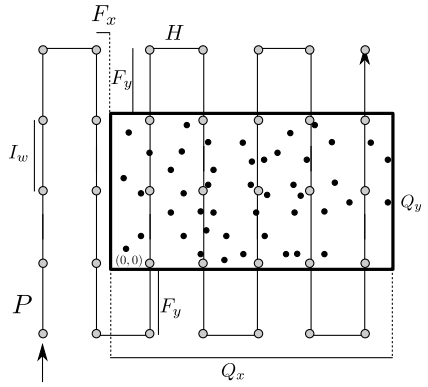

Figure 5: The static path $\mathcal{D}$ and the deployment area Q.

is at distance no larger than $\lfloor \frac{d_{max}-2I_w}{2} \rfloor$ from the rightmost vertical border of the deployment area Q.

For each node, we select the three waypoints in two consecutive vertical scans, to avoid the "alias" problem due to waypoints collinearity. To limit the selection of the three waypoints to two consecutive vertical scans, we assume $H \geq \frac{d_{min}}{2}$. Therefore, we add the constraint:

$$d_{min} < \frac{d_{max}}{2} - I_w. \quad (7)$$

3.3 Tessellation and Ranging Waypoints

In this section, we explain how to select on $\mathcal{D}$ the ranging waypoints that correctly measure each possible node in Q.

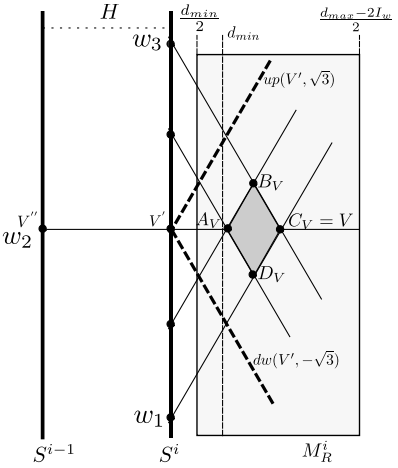

Figure 6: The tessellation and, in gray, the stripe M_R^i measured by the vertical scans S_i and S_{i-1}.

Let the vertical scans in $\mathcal{D}$ be numbered from 0 to ν. Consider on $\mathcal{D}$ two consecutive vertical scans S^{i-1} and S^i, with $1 \leq i \leq \nu$. Let x_{S^i} be the x-coordinate of the vertical scan S^i of $\mathcal{D}$. In the following, we prove that the points of Q on the right of S^i whose x-coordinate belong to the interval $\left[x_{S^i} + \frac{d_{min}}{2}, x_{S^i} + \frac{(d_{max}-I_w)}{2}\right]$ form the stripe of Q, named M_R^i and illustrated in Fig. 6, that can be correctly measured from S^{i-1} and S^i.

To decide how to associate the waypoints on S^i and S^{i-1} with the nodes in Q, we logically tessellate M_R^i as follows. From every even waypoint $w = (x_w, y_w) = (x_w, 2tI_w)$ on S^i, with $0 \leq t \leq \lceil \frac{L}{2I_w} \rceil$, we draw the two lines that pass through w with slope $m_1 = \sqrt{3}$ and $m_2 = -\sqrt{3}$ denoted, respectively, as $up(w, m_1)$ and $dw(w, m_2)$ (see Fig. 6). Such lines design a lattice on M_R^i, made of diamond shapes. Each vertex of the lattice is uniquely associated with the diamond on its left. Precisely, consider the vertex $V = C_V = (x_V, y_V)$ in Fig. 6. It is associated with the diamond $\Delta(V)$ (displayed in dark gray) of vertices (listed in clockwise order starting from V): $C_V = V$, $D_V = \left(x_V - \frac{I_w}{\sqrt{3}}, y_V - I_w\right)$, $A_V = \left(x_V - 2\frac{I_w}{\sqrt{3}}, y_V\right)$, and $B_V = \left(x_V - \frac{I_w}{\sqrt{3}}, y_V + I_w\right)$. Observe that all the diamond shapes of the tessellation have the same size. For every diamond $\Delta(V)$, the horizontal diagonal $A_V C_V$ has length $|A_V C_V| = \frac{2I_w}{\sqrt{3}}$ while the vertical diagonal $B_V D_V$ has length $|B_V D_V| = 2I_w$. Moreover, the projections V' and V'' of V are waypoints on S^i and S^{i-1} because their y-coordinate is multiple of I_w.

Let V be at the intersection of the lines $up(V_S, \sqrt{3})$ and $dw(V_N, -\sqrt{3})$. V_S and V_N play a very important role in our localization technique, along with the projection V' of V on S^{i-1}: Indeed, $w_1(P) = V_S$, $w_2(P) = V'$, and $w_3(P) = V_N$ for each P in the diamond $\Delta(V)$, represented by V.

THEOREM 1. *Fixing the vertex $V = (x_V, y_V) \in M_R^i$ that occurs at the intersection of the lines $up(V_S, \sqrt{3})$ and $dw(V_N, \sqrt{3})$, the nodes in $\Delta(V)$ are correctly measured by the ranging waypoints V_S, V_N and the projection V'' of V on S^{i-1}.*

PROOF. Fix $w_1(P) = V_S$, $w_2(P) = V''$, and $w_3(P) = V_N$. First observe that since V occurs at the intersection of the lines $up(V_S, \sqrt{3})$ and $dw(V_N, -\sqrt{3})$, by elementary geometric arguments it holds that $d(V_S, V) = d(V_N, V) = 2d(V', V) = 2(x_V - x_{S^i})$, where V' is the projection of V on S^i. Thus, recalling that V belongs to the stripe M_R^i on the right of S^i that is, $\frac{d_{min}}{2} \leq x_V - x_{S^i} \leq \frac{(d_{max}-2I_w)}{2}$, it immediately follows that

$$d_{min} \leq d(w_1(V), V) \leq d_{max} - 2I_w.$$

Moreover, it holds $d_{min} < H + \frac{dmin}{2} < d(w_2(V), V) \leq H + \frac{d_{max}-2I_w}{2} < d_{max}$. Thus, the d_{min} and d_{max} constraints are satisfied for V.

To prove the d_{min} and d_{max} constraints for each internal node $P \in \Delta(V)$, let us first consider each node P in the lower half-diamond $\Delta(V)$, that is, the triangle $A_V C_V D_V$ of $\Delta(V)$. Let P' be the projection of P on S^i and let $\widehat{P'V_SP}$ be the angle at V_S between the ray V_SP and the vertical scan S^i. Since $d(V_S, P') \leq d(V_S, V')$ because P belongs to the triangle $A_V D_V C_V$ and $\widehat{P'V_SP} \leq \widehat{V'V_SV}$, it holds that:

$$d(w_1(V), P) = \frac{d(w_1(V), P')}{\cos(P'w_1(V)P)} \leq \frac{d(w_1(V), V')}{\cos(P'w_1(V)P)} \leq \frac{d(w_1(V), V')}{\cos(V'w_1(V)V)} = d(w_1(V), V) \leq d_{max} - 2I_w.$$

Moreover, for each P in the triangle $A_V B_V C_V$ of $\Delta(V)$, consider the point P'' symmetric to P with respect to the line $V'V$ which belongs to the triangle $A_V D_V C_V$.

By the triangle inequality, given that V belongs to M_R^i and $d(P'', P) \leq d(B, D)$, we have:

$$d(w_1(V), P) \leq d(w_1(V), P'') + d(P'', P) \leq d(w_1(V), P'') + 2I_w \leq d(w_1(V), V) + 2I_w \leq d_{max}$$

Repeating the same reasoning, using $w_3(P) = V_N$ in place of $w_1(P) = V_S$, it can be proved that for each $P \in \Delta(V)$, it holds $d_{min} \leq d(V_N, P) \leq d_{max}$.

With regard to the d_{min} and d_{max} constraints for $w_2(P)$, let Z be the projection of $P \in \Delta(V)$ on the diamond diagonal AC. It easily follows that $d(w_2(V), P) \leq d(w_2(V), Z) + d(Z, P) \leq d(w_2(V), V) + I_w < H + \frac{d_{max}}{2} - I_w < d_{max}$, and $d(w_2(V), P) \geq d(w_2(V), Q) \geq H + \frac{d_{min}}{2} > d_{min}$ because $H > \frac{d_{min}}{2}$.

For the β_{min} constraint in vertex V, observe that the tessellation divides the turn angle in V in equal angles. Therefore, $\beta(V) = \frac{\pi}{3}$. Since $\tan(\frac{\beta(V)}{2}) = \frac{1}{\sqrt{3}}$, the β_{min} constrained is satisfied.

In each diamond $\Delta(V)$,$\min_{P \in \Delta(V)} \beta(P) = \beta(A_V)$. Then,

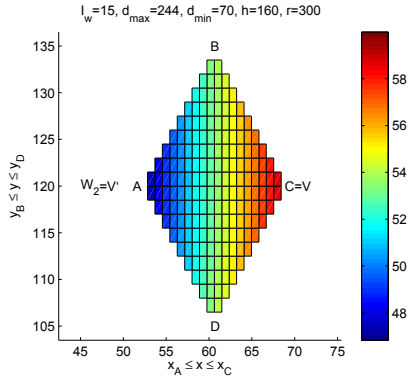

Figure 7: The angular aperture $\beta(P)$ for $P \in \Delta(V)$ with V at distance $70m$ from a vertical scan S ($x_S = 0$) and $I_w = 15m$.

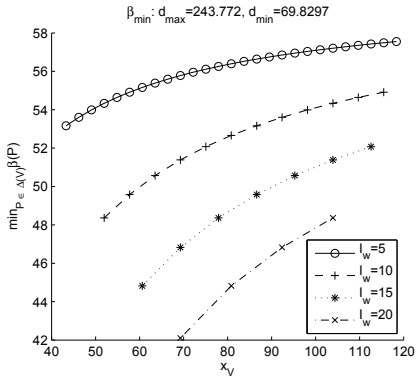

Figure 8: The width of $\beta(A_V) = \min_{P \in \Delta(V)} \beta(P)$ versus the x-coordinate of the representative vertex V.

for each $P \in M_R^i$, β_{min} occurs at the vertex A_V with minimum x-coordinate. Moreover, $\frac{\beta_{min}}{2} = \tan^{-1}\left(\frac{\frac{d_{min}}{2}}{\sqrt{3}\frac{d_{min}}{2}+2I_w}\right)$.

Figure 7 illustrates the width of the angle $\beta(P)$ in a diamond shape of M_R^i and gives evidence that $\beta(A_V) = \min_{P \in \Delta(V)} \beta(P)$. Figure 8 shows the fact that increasing the distance of V from S^i, $\beta(A_V)$ increases.

Since we proved that from S^{i-1} and S^i the nodes in M_R^i are correctly measured, considering all the pairs of consecutive scans (S^0,S^1), (S^1,S^2) ... $(S^{\nu-1},S^\nu)$ we cover $\cup_{i=1}^{\nu} M_R^i = Q$. Hence, all the nodes in Q can be correctly measured from the vertical scans $S^0, \ldots, S^\nu$. □

3.4 The Localization Mission

In this section, we describe the drone's behaviour. The drone follows the path $\mathcal{D}$, and at each waypoint it sends a message beacon. The non-localized nodes that can hear it reply with an ack message to the drone. From the round-trip time, the drone can infer the slant distance between itself and the node, and from that, it computes the ground distance. The drone locally saves all the ground distance measurements for the nodes not yet localized.

For each node P, the drone first finds a rough estimate (without any guaranteed bound on the position error), called $\hat{P}$, of the position of the node P. Then, the drone locates the logical diamond $\hat{\Delta}$ where $\hat{P}$ resides, and uses the

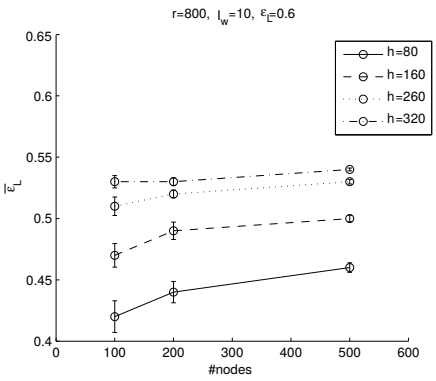

Figure 10: The precision $\bar{\epsilon}_L$ when $r = 800m$ for different altitudes when $\epsilon_L = 0.6m$.

three ranging waypoints associated to $\hat{\Delta}$ to localize P with guaranteed bound precision ϵ_L.

Precisely, to compute $\hat{P}$, the drone performs a trilateration with the first three distance measurements it collects that satisfy the d_{min} constraint and that belong to two different vertical scans. From $\hat{P}$, it locates the closest vertical scan $S^{\sigma(\hat{P})}$, with index $\sigma(\hat{P}) = \left\lfloor \frac{x_{\hat{P}}+F_x}{H} \right\rfloor + 1$, on the left of $\hat{P}$. Then, based on the distance between $S^{\sigma(\hat{P})}$ and $\hat{P}$ the drone computes $w_1(\hat{P}), w_2(\hat{P}), w_3(\hat{P})$. Let:

$$\bar{y_1} = \left\lfloor \frac{y_{\hat{P}}}{2I_w} - \left\lceil \frac{\sqrt{3}(x_{\hat{P}} - x_{S^{\sigma(\hat{P})}})}{2I_w} \right\rceil \right\rfloor 2I_w$$

$$\bar{y_3} = \left\lfloor \frac{y_{\hat{P}}}{2I_w} + \left\lceil \frac{\sqrt{3}(x_{\hat{P}} - x_{S^{\sigma(\hat{P})}})}{2I_w} \right\rceil \right\rfloor 2I_w$$

$$\bar{y_2} = \frac{(\bar{y_1} + \bar{y_3})}{2}$$

Then, if $x_{S^{\sigma(\hat{P})}} \leq x_{\hat{P}} \leq x_{S^{\sigma(\hat{P})}} + \frac{d_{min}}{2}$, the drone will again trilaterate P after the distance measurements at the three ranging points:

$$\begin{aligned} w_1(\hat{P}) &= \left(x_{S^{\sigma(\hat{P})-1}}, \bar{y_1}\right) \\ w_2(\hat{P}) &= \left(x_{S^{\sigma(\hat{P})-2}}, \bar{y_2}\right) \\ w_3(\hat{P}) &= \left(x_{S^{\sigma(\hat{P})-1}}, \bar{y_3}\right) \end{aligned} \tag{8}$$

Similarly, if $x_{S^{\sigma(\hat{P})}} + \frac{d_{min}}{2} < x_{\hat{P}} \leq x_{S^{\sigma(\hat{P})+1}}$, the localization will be completed as soon as the drone has collected the distance measurements from the waypoints:

$$\begin{aligned} w_1(\hat{P}) &= \left(x_{S^{\sigma(\hat{P})}}, \bar{y_1}\right) \\ w_2(\hat{P}) &= \left(x_{S^{\sigma(\hat{P})-1}}, \bar{y_2}\right) \\ w_3(\hat{P}) &= \left(x_{S^{\sigma(\hat{P})}}, \bar{y_3}\right) \end{aligned} \tag{9}$$

In both cases, the localization of P will now satisfy the bound ϵ_L since the three waypoints satisfy the d_{min}, d_{max}, and β_{min} constraints.

In the next section we confirm our results by simulations.

4. EXPERIMENTAL EVALUATION

We have implemented the localization technique in Matlab. We simulate a localization mission by deploying at

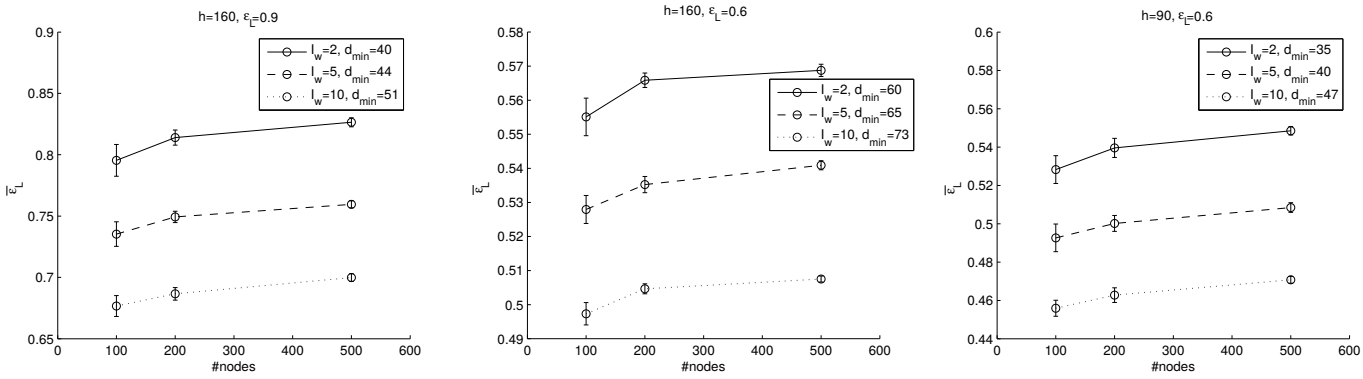

(a) (b) (c)

Figure 9: The precision $\bar{\epsilon}_L$ when $r = 300m$.

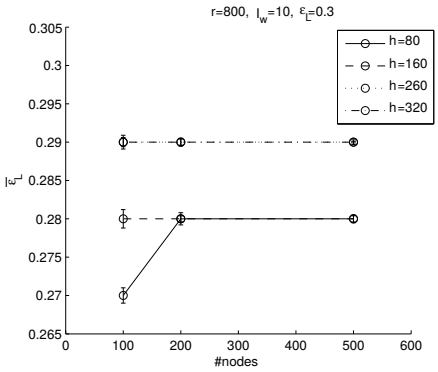

Figure 11: The precision $\bar{\epsilon}_L$ when $r = 800m$ for different altitudes when $\epsilon_L = 0.3m$.

random a variable number n of nodes, with $n = 100, 200$ and 500, on a $1000m \times 1000m$ map. In all experiments, the drone travels along the path $\mathcal{D}$ and takes distance measurements at the waypoints. We assume the slant precision to be $\epsilon_s = 0.1m$, as claimed by DecaWave for their IR-UWB transceivers [1]. To simulate the slant distance between the drone in position w at altitude h and the node P, we compute the exact slant distance (without error) $s = \sqrt{|wP|^2 + h^2}$, where $|wP|$ is the Euclidean (exact) distance between the projection of w on the ground and the (exact) position of P. Then we generate a slant error $e_s \in [-\epsilon_s, \epsilon_s]$ and we say that the slant distance measured by the drone is $s(w, P) = (s+e_s)$. The ground distance (which includes the ground error) is computed as $d(w, P) = \sqrt{s(w, P)^2 - h^2}$. Given three ground measures, the estimate position of P is computed as the least-squares-error solution of their trilateration.

For every tuple $(r, h_{max}, d_{max} I_w, \epsilon_L)$ reported in Table 2, we generate 35 different localization missions. For each tuple, we derive by Eq. 6 the value of d_{min} required to satisfy the given ϵ_L. If such a value d_{min} does not satisfy Eq. 7, our localization technique cannot achieve ϵ_L, unless we decrease the value of I_w. Fixing n, for each mission, we simulate the localization technique. We assume that the drone flies at altitude $h = h_{max}$ or lower. Note that if the actual altitude is smaller than h_{max} , the localization precision improves.

In order to evaluate the localization precision obtained during the simulated mission, we evaluate the *experimental position precision* $\epsilon_L(P)$ for each node P. Formally, if P is measured by w_1, w_2 and w_3, we compute:

$$\epsilon_L(P) = \epsilon_s \frac{\sqrt{1 + \frac{h_{max}^2}{\min_{i=1}^{3}\{d^2(w_i, P)\}}}}{\frac{\beta(P)}{2}}. \quad (10)$$

For each mission M, we record the *worst experimental localization precision*, that is, $\epsilon_L(M) = \max_{P \in Q}(\epsilon_L(P))$. Then, we compute the *average of the worst experimental localization precision* $\bar{\epsilon}_L = \frac{\sum_{i=1}^{35} \epsilon_L(M_i)}{35}$. In our experiments we are interested in comparing ϵ_L with $\bar{\epsilon}_L$.

r (m)	h_{max} (m)	d_{max} (m)	I_w (m)	ϵ_L (m)
300	160	254	$[2, 5, 10]$	$[0.9, 0.6]$
300	90	286	$[2, 5, 10]$	$[0.6, 0.3]$
800	160	784	$[2, 5, 10]$	$[0.6, 0.3]$
800	90	795	$[2, 5, 10]$	$[0.6, 0.3]$

Table 2: Values of the parameters used to generate the localization missions. All the measures are expressed in meters.

As shown in Fig. 9, the desired localization precision is always greater than the average worst experimental localization precision. Not only, $\bar{\epsilon_L} \leq \epsilon_L$, but also $\epsilon_L(M) \leq \epsilon_L$ for each individual mission. The distance between the desired value ϵ_L and the experimental $\bar{\epsilon}_L$ increases when d_{min} increases and I_w increases. So the experiments guarantee a better (i.e., smaller) localization precision when d_{min} is larger.

When $h = 160m$ and $\epsilon_L = 0.6m$, d_{min} is greater than when $h = 90m$ and $\epsilon_L = 0.6m$. In other words, a larger d_{min} is required to achieve the same ϵ_L at higher altitudes (see Fig. 9b and 9c). This shows that the experimental localization precision is sensitive to the altitude.

For $h_{max} = 160m$ and $r = 300m$, it is not possible – with the current localization technique – to guarantee $\epsilon_L = 0.3m$ since d_{min} violates Eq. 7. The same precision can be achieved with larger communication ranges or smaller altitudes (see Table 2).

Figs. 10 and 11 plot the precision $\bar{\epsilon}_L$ for $r = 800m$ at different altitudes when the a-priori localization precision to be guaranteed is $\epsilon_L = 0.6$ and $\epsilon_L = 0.3$, respectively. Although the distance between the theoretical and the experimental precisions decreases when h increases, the experimental localization precision is always smaller than ϵ_L.

In order to compare our localization technique with previously known localization algorithms, we evaluate in Fig. 12 the localization precision for the LMAT localization algorithm proposed in [10] when the transmission radius is equal to $d_{max} = 254m$. The ranging waypoints are selected as in LMAT. In other words, the d_{min} constraint is not verified, while the collinearity with the node is low due to the way LMAT selects the ranging waypoints. As before, we execute 35 missions. As one can note, $\bar{\epsilon}_L$ is always greater than $500m$. This is due to the fact that the ground precision becomes very large because $d(w, P)$ can be very very small. To avoid such extreme cases, we also computed the average position error among all the experimental localization precision (not only the worst precision) of each mission. Still, that value remains above $8m$, which is more than 10 times the precision guaranteed by our technique.

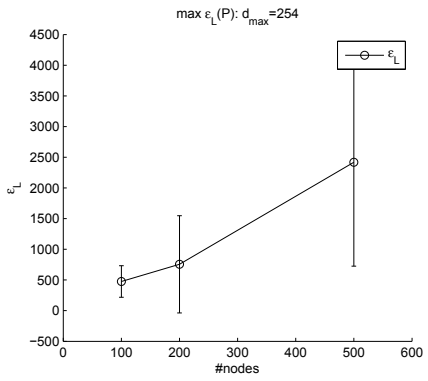

Figure 12: The error bound $\bar{\epsilon}_L$ in the LMAT algorithm [10].

5. CONCLUSION

In this paper, we presented a localization technique that replaces multiple anchors with a flying drone. Our solution guarantees a provable bound on the position error by tuning a single parameter: the minimum ground distance measurement. During the localization mission, the drone first computes for each sensor a rough estimation of its position, and then it carefully selects the waypoints so as the required localization precision is guaranteed. As a future work, we intend to consider a drone equipped with directional antennas in order to avoid the rough estimation of each point and to extend our technique for localizing nodes in 3D.

6. REFERENCES

[1] DecaWave, ScenSor SWM1000 Module.

[2] Bhadauria, D., Tekdas, O., and Isler, V. Robotic data mules for collecting data over sparse sensor fields. *J. of Field Robotics 28*, 3 (2011), 388–404.

[3] Caballero, F., Merino, L., Gil, P., Maza, I., and Ollero, A. A probabilistic framework for entire {WSN} localization using a mobile robot. *Robotics and Autonomous Systems 56*, 10 (2008), 798–806. Network Robot Systems.

[4] Corke, P., Peterson, R., and Rus, D. Coordinating aerial robots and sensor networks for localization and navigation. In *Distributed Autonomous Robotic Systems 6* (2007), Springer Japan, pp. 295–304.

[5] Dang, P., Lewis, F. L., and Popa, D. O. Dynamic localization of air-ground wireless sensor networks. In *MED'06* (2007), Springer, pp. 431–453.

[6] Ergezer, H., and Leblebicioglu, K. Path planning for UAVs for maximum information collection. *IEEE Trans. on Aerospace and Electronic Systems 49*, 1 (2013), 502–520.

[7] Han, G., Xu, H., Duong, T. Q., Jiang, J., and Hara, T. Localization algorithms of Wireless Sensor Networks: a survey. *Telecommunication Systems 52*, 4 (2013), 2419–2436.

[8] Heredia, G., Caballero, F., Maza, I., Merino, L., Viguria, A., and Ollero, A. Multi-unmanned aerial vehicle (UAV) cooperative fault detection employing differential global positioning (DGPS), inertial and vision sensors. *Sensors 9*, 9 (2009), 7566–7579.

[9] Huang, R., and Zaruba, G. V. Static path planning for mobile beacons to localize sensor networks. In *Pervasive Computing and Communications Workshops, 2007. PerCom Workshops '07* (March 2007), pp. 323–330.

[10] Jiang, J., Han, G., Xu, H., Shu, L., and Guizani, M. Lmat: Localization with a mobile anchor node based on trilateration in wireless sensor networks. In *Global Telecommunications Conference (GLOBECOM 2011), 2011 IEEE* (Dec 2011), pp. 1–6.

[11] Mtawa, Y. A., Nasser, N., and Hassanein, H. S. Mitigating anchor misplacement errors in wireless sensor networks. In *2015 International Wireless Communications and Mobile Computing Conference (IWCMC)* (Aug 2015), pp. 569–575.

[12] Pathirana, P. N., Bulusu, N., Savkin, A. V., and Jha, S. Node localization using mobile robots in delay-tolerant sensor networks. *IEEE Trans. on Mobile Computing 4*, 3 (2005), 285–296.

[13] Perazzo, P., Ariyapala, K., Conti, M., and Dini, G. The Verifier Bee: A path planner for drone-based secure location verification. In *WoWMoM'15* (2015), pp. 1–9.

[14] Pinotti, C., Betti Sorbelli, F., Perazzo, P., and Dini, G. Localization with guaranteed bound on the position error using a drone. *Tech. Rep., University of Perugia* (2016).

[15] Schleich, J., Panchapakesan, A., Danoy, G., and Bouvry, P. Uav fleet area coverage with network connectivity constraint. In *MobiWac '13* (2013), pp. 131–138.

[16] Shioda, S., and Shimamura, K. Cooperative localization revisited: Error bound, scaling, and convergence. In *MSWiM '13* (2013), pp. 197–206.

[17] Ssu, K.-F., Ou, C.-H., and Jiau, H. C. Localization with mobile anchor points in wireless sensor networks. *IEEE Transactions on Vehicular Technology 54*, 3 (May 2005), 1187–1197.